

Sustainable, Dendrite Free Lithium-Metal Electrode Cycling Achieved with Polymer Composite Electrolytes Based on a Poly(Ionic Liquid) Host

Gaetan M. A. Girard,^[a] Xiaoen Wang,^[a] Ruhmah Yunis,^[a] Douglas R. MacFarlane,^[b] Aninda J. Bhattacharyya,^[c] Maria Forsyth,^[a] and Patrick C. Howlett^{*[a]}

Polymer composite solid-state electrolyte materials based on ionic liquids stand out as viable alternatives to flammable liquid electrolytes for solid state lithium-metal batteries. They offer a compromise between favourable mechanical properties and stability against Li-metal, coupled with favourable ion transport. However, insufficient Li^+ transport properties for practical battery operation may result from the higher mobility of other ionic species from the ionic liquid (IL). Here, this issue was addressed by confining a highly concentrated IL electrolyte in a poly(ionic liquid) matrix with the addition of 5 wt% of alumina nanoparticles; these superconcentrated IL electrolytes favour Li^+ ion transport. The composites are based on a poly(diallyldimethylammonium) bis(trifluoromethanesulfonyl)imide

(PDADMA NTf_2) matrix, and an electrolyte solution (ES) of high lithium concentration phosphonium IL, trimethyl(isobutyl) phosphonium bis(fluorosulfonyl)imide ($\text{P}_{1114}\text{FSI}$), with 3.8 mol kg^{-1} (3.8 M) LiFSI . The impact of ES content within the composite on Li^+ transference number and electrochemical stability against Li-metal is reported. For the 50 wt% ES and 50 wt% of PDADMA NTf_2 composite, up to 0.5 mAh cm^{-2} of Li-metal plating/stripping for over 20 days at 50°C is shown. Scanning electron microscopy (SEM) confirmed that no Li dendrite formation was visible at the Li-metal/polymer composite interface. Competitive performance of LiFePO_4 electrodes (1.2 mAh cm^{-2}) is also reported.

1. Introduction

High ionic conductivity that describes high ion mobility in solid electrolytes has long been sought for advanced high energy density lithium (Li) metal batteries.^[1–4] The aim is to obtain a solid material with liquid-like ion transport properties. One approach is to plasticise a polymer matrix via immobilising an ionic liquid (IL) solution inside the polymer,^[5] which is referred to as a polymer composite electrolyte. Achieving favourable dimensional stability without compromising ion transport properties within the material remains a challenge for the use of polymer composites in advanced batteries. Ion transport in these composites is unique and under continuous investigation.^[6] It differs from the ion conduction mechanism in conventional electrolytes.^[7] The ion mobility is decoupled from the polymer chain and believed to be dictated by the dynamics and solvation properties of confined liquids.^[6] The interactions between the ions and the polymer host have a strong influence

on the composites' macroscopic (e.g., liquid-like or solid-like by tailoring the IL:polymer ratio) and transport properties.^[8] By tuning both the polymer structure and chemical composition, the physicochemical properties of the composite material can be tailored.^[9–10] The use of a plasticiser facilitates the polymer matrix relaxation while maintaining mechanical integrity and strength suitable for battery fabrication.

For their unique properties, ionic liquids (ILs) are suitable materials to act as plasticisers for the fabrication of novel composites whilst also contributing to ionic conductivity.^[6,11–12] Le Bideau et al. studied Li^+ transport in *N*-methyl-*N*-propylpyrrolidinium bis(trifluoromethanesulfonyl)imide ($\text{C}_3\text{mpyr }\text{NTf}_2$) confined in silica monoliths.^[13] An optimum mesopore diameter, 10 nm, for an optimum concentration of 0.5 M LiNTf_2 was reported for which Li transport was greater in comparison to that of the bulk IL.

Polymerised ionic liquids, also referred to as polyILs or poly(ionic liquids), have recently received great interest as alternative polymer host networks for novel polymer composites.^[14–17] The choice of poly(diallyldimethylammonium) bis(trifluoromethanesulfonyl)imide, PDADMA NTf_2 , or often called poly(DDA) NTf_2 , is arising due to its low cost and remarkable chemical affinity with ILs. Free-standing membranes presenting an anodic stability above 4.5 V vs. Li^+/Li at 40°C and high ionic conductivity at 60°C ($\approx 10^{-3} \text{ S cm}^{-1}$) were successfully reported.^[18] The presence of mixed anions, NTf_2^- and bis(fluorosulfonyl)imide FSI^- , helped reduce the interfacial resistance of Li-metal and improve electrolyte oxidation stability.^[17] Polycations also remarkably enhanced Li^+ diffusivity for medium to low Li salt concentrations for which the final

[a] Dr. G. M. A. Girard, Dr. X. Wang, Dr. R. Yunis, Prof. M. Forsyth, Prof. P. C. Howlett

Institute for Frontier Materials

Deakin University

Burwood, VIC 3125, Australia

E-mail: patrick.howlett@deakin.edu.au

[b] D. R. MacFarlane

School of Chemistry

Monash University

Clayton, VIC 3800, Australia

[c] Prof. A. J. Bhattacharyya

Solid State and Structural Chemistry Unit

Indian Institute of Science

Bangalore 560012, India

viscosity of the liquid phase is lower, presumably increasing transference number.^[19]

In the majority of studies reported to date in the area of solid state Li batteries, the applied current densities used have been limited to $0.1\text{--}0.5\text{ mA cm}^{-2}$.^[4,20\text{--}22] Previous reports have addressed acceptable performance of Li-metal in a gel polymer electrolyte based on imidazolium bis(trifluoromethanesulfonyl) imide, EMI NTf₂, with reversible cycling at a current density of 0.36 mA cm^{-2} .^[21] Additional benefits of the incorporation of ILs into a poly(vinylidene fluoride-cohexafluoropropylene):silica matrix (PVDF-HFP:SiO₂), such as an increased compatibility with the Li anode suppressing the growth of lithium dendrites and lowering the SEI resistance, were recently emphasised.^[20] A solution of 1-ethyl-3-methylimidazolium trifluoromethanesulfonate/ethylene carbonate/propylene carbonate, EMI NTf₂/EC/PC, was used at different ratios with up to 75 wt% of EMI NTf₂.^[20]

In our recent report, an effective strategy to improve the lithium ion transport in concentrated polymer composite electrolytes by incorporation of a highly concentrated ionic liquid solution into a polyIL host network was described.^[14] We showed that the introduction of high lithium-concentration ionic liquids into the polyIL effectively decreased the glass transition temperature (T_g) of the resulting composites, improved ion dynamics with increasing Li⁺ ion mobility and NTf₂⁻/FSI⁻ anion exchange and resulting in higher ionic conductivity. The addition of alumina, Al₂O₃, nanoparticles also enhanced the mechanical integrity of the free-standing films which exhibited stable Li-metal symmetrical cycling (over 200 h at 0.05 mA cm^{-2} and 0.05 mAh cm^{-2}). A fixed amount of LiFSI was used in the electrolyte solution (ES): 3.8 mol kg^{-1} (3.8 m) is the maximum amount of Li salt that can be dissolved into the phosphonium IL (P₁₁₁₁₄ FSI). The phosphonium based IL was employed due to enhanced electrochemical, ion transport and thermal properties when compared to the more widely studied *N*-based ILs, they are also becoming more widely available and attracting research interest as high stability electrolytes.^[23\text{--}27] The high concentration solution was chosen due its advantages (compared to the dilute electrolyte) of higher rates of Li transport, improved SEI properties and enhanced cycling performance of the lithium-metal anode.^[25,28\text{--}29]

Here we demonstrate a significant ability of plating/stripping lithium-metal in these polymer composites. Highly stable plating/stripping is shown in a selected composite with extensive amounts of charge plated/stripped, up to 0.5 mAh cm^{-2} . The interface between the Li-metal and the polymer composite was characterised by electrochemical impedance spectroscopy (EIS) and scanning electron microscopy (SEM).

The impact of an increase of ES on the cycling performance of Li-metal electrodes is also discussed. Finally, the performance of lithium iron phosphate electrodes, LiFePO₄, with areal capacity of 1.2 mAh cm^{-2} at a C/15 rate is reported and revealed to be competitive with latest solid electrolyte systems. The phosphoolivine compound LiFePO₄ was chosen for its low cost, low toxicity, high thermal stability and high specific capacity of 170 mAh g^{-1} . Iron metal (Fe) is also abundant, inexpensive, and less toxic than other metals (e.g., Co, Ni, or Mn).^[30]

2. Results and Discussion

2.1. Determination of Lithium Transference Number

Lithium transference number and ionic conductivity are critical factors when considering the application of electrolyte materials in batteries. Table 1 provides the values for the composite compositions reported here. When a symmetric cell is polarised, all positive ions (in this case, Li⁺ and P₁₁₁₁₄⁺ cations) move in the direction of the negatively polarised electrode, while negative ions (NTf₂⁻ and FSI⁻) move towards the positively polarised electrode. Figure 2a displays the values of lithium transference number, t_{Li}^+ , with increasing ES ratio (30, 40 and 50 wt%) including error bars. The values confirm slower kinetics and unique lithium transport in the polymer composite electrolytes in comparison with the pure liquid electrolyte solution (ES). However, the transference number shifts to higher values as the ES content in the electrolyte is increased. Among the composite materials reported here, the highest transference number of 0.18 ± 0.02 was obtained with 50 wt% ES. This implies that the fraction of current transported by the Li⁺ cation within the electrolyte is the highest for this concentration. It should be mentioned that there is a direct correlation between the assumptions made (i.e., the equation used for the calculation of t_{Li}^+) and the final values. For example, Suo et al. assume that the cell resistance remains constant during the polarisation and values up to 0.7 were reported for a highly concentrated ether-based liquid electrolyte.^[31] In our case, if the same assumptions were made, the values would increase and 0.30 ± 0.03 would be reported with 50 wt% ES.

Ideally, electrolytes with $t_{\text{Li}}^+ \approx 1$ and good ion-pair dissociation are desirable as they may delay the nucleation of Li dendrite and improve Li plating in rechargeable batteries with metallic Li anodes.^[32\text{--}33] Transference numbers in the composites with high Li salt content reported here are still significant.

Table 1. Molar composition and properties of the studied polymer composite electrolytes.

Electrolyte solution (ES)	ES/PDADMA ratio [wt%]	Polymer composite name	Molar ratio PDADMA NTf ₂	Li FSI	P ₁₁₁₁₄ FSI	$\sigma^{[a]}$ [S cm ⁻¹]	$t_{\text{Li}}^+ {[b]}$
$\text{P}_{11114}\text{ FSI} + 3.8\text{ m LiFSI}$	100/0	3.8 mol kg^{-1} LiFSI in IL	—	0.55	0.45	9.6×10^{-4}	0.59 ± 0.02
	40/60	40/60-Al ₂ O ₃	0.47	0.29	0.24	8.6×10^{-5}	0.08 ± 0.02
	50/50	50/50-Al ₂ O ₃	0.38	0.34	0.28	2.8×10^{-4}	0.18 ± 0.02

[a] Ionic conductivity measured at $T = 30^\circ\text{C}$ ^[14] [b] Transference number measured at $T = 50^\circ\text{C}$

Guyomard et al. recently reported a comparable transference number of ca. 0.15, at a lower temperature (25 °C), for an ion gel based on lower LiNTf₂ content (0.5 M) and C₃mpyr NTf₂ confined in a silica mesoporous network.^[13] The values of the Li⁺ transference numbers reported here and acquired by the direct electrochemical method at 50 °C are different from those acquired by PFG-NMR measurement (at 60 °C), indeed they are lower (0.08 vs. 0.40 for the 40/60-Al₂O₃ electrolyte, and 0.18 vs. 0.32 for the 50/50-Al₂O₃ electrolyte).^[14] This phenomenon has previously been described.^[34] It is speculated that the polarisation bias can strongly influence ion transfer, formation of the electrical double layer and influence the mechanism of SEI formation on the surface of the electrode. A diffusion technique such as PFG-NMR, is purely nuclei sensitive and does not respond to an electric field, therefore the flux of both ion pairs and free ions is measured and gives a 'pseudo' transference number.^[35] In our previous work we found that the addition of PDADMA NTf₂ to the polymer composite decreased the diffusion coefficient of both Li⁺ and anions.^[14]

Exemplary data set of the polarisation profile of a symmetric cell containing the 50/50-Al₂O₃ composite electrolyte for 4 hours is shown in Figure 2b. The cells reached a steady state current within one hour, however the polarisation was maintained for 4 hours to obtain consistent results as previously reported with other polymers (e.g., PEO) or plastic crystal electrolytes, which require several hours to reach a steady state current.^[36] The Li surface resistances are represented in the Nyquist plots, Figure 2c. To determine the resistances of passivation layers before and after polarisation, the equivalent circuit proposed in Figure 2d was used. The electrolyte resistance remains stable and oscillates between 57 and 52 Ω·cm² (before and after steady state respectively) while the Li surface resistance decreases from approximately 202 to 174 Ω·cm². The shift of the semicircle towards lower impedance indicates that the interfacial resistance was reduced, indicating that the passivating layer on the Li surface became less resistive after electrode polarisation.

2.2. Influence of the Ionic Liquid Content on Cycling Performance of Lithium-Metal

Galvanostatic cycling measurements using symmetric lithium-metal cells are routinely conducted in order to investigate the ability of a given electrolyte to sustain efficient plating and stripping of Li-metal, in this case, and the effect of rate applied (i.e., current density) on the stability of this electrochemical process. The interface stability was measured by galvanostatic 'charging' and 'discharging' at a constant current to plate and strip Li⁺ cation.

Figure 3 shows the time-dependent voltage profile of the Li|Li symmetric cells with the two polymer composites at a current density of 0.1 mA cm⁻² at 50 °C. Positive and negative potentials correspond to Li-metal plating and stripping respectively. With both composites the first Li plating process starts with a smooth steady increase in the potential. This observation indicates that a smooth interphase on the Li-metal electrode is formed post cell assembly. It is important to note that the polarisation reached at the end of the first process is lower in the case of the 50/50-Al₂O₃ electrolyte and the values are discussed below. The shape of the voltage profile curve and value of the potential reached at the end of each process are known to be fingerprints of any surface rearrangements occurring on the Li-metal electrode.^[28,37] The observations from the present experiments already suggest that the IL content in the polymer composite has an impact on the interfacial resistance. An increase of IL content seems to promote a good interfacial contact between the electrode and the electrolyte associated with a smooth Li-metal surface and low resistance interphase. This implies that higher current rates, i.e., amount of Li plated/stripped, can be applied with the composite 50/50-Al₂O₃. The slight increase in potential over the first 25 cycles, for which the maximum polarisation in the whole experiment is reached, can be explained by a specific kinetic hindrance for Li plating underneath the native surface film on the electrode and the SEI formed spontaneously after contact with the polymer composite post-assembly. The potential stabilises very rapidly after this initial cycling in both cases.

The cell with 50/50-Al₂O₃ electrolyte exhibited (Figure 3a) a low and very stable voltage (\approx 0.08 V at the first and 50th plating) for Li plating and a low voltage (\approx -0.08 V at the first

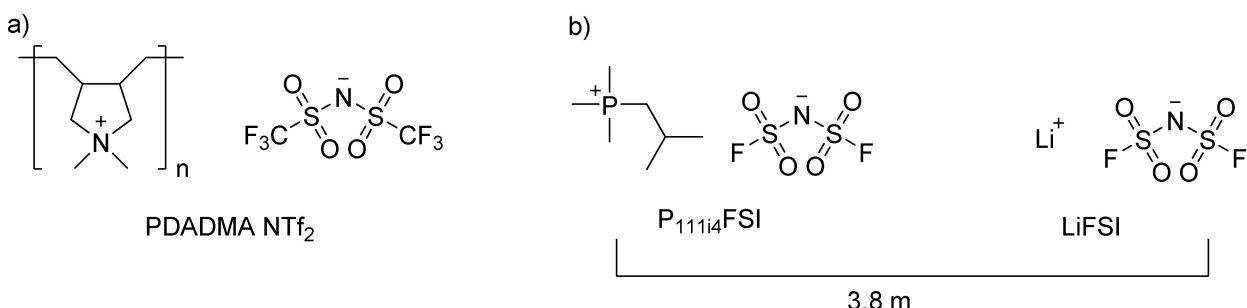


Figure 1. Chemical structure of polymer composite electrolyte components: a) poly(diallyldimethylammonium) bis(trifluoromethanesulfonyl)imide, PDADMA NTf₂ and b) electrolyte solution (ES) based on trimethyl(isobutyl)phosphonium bis(fluorosulfonyl)imide, P₁₁₁₁₄FSI, and lithium bis(fluorosulfonyl)imide, LiFSI. ES: 3.8 m (mol kg⁻¹) LiFSI dissolved into P₁₁₁₁₄FSI.

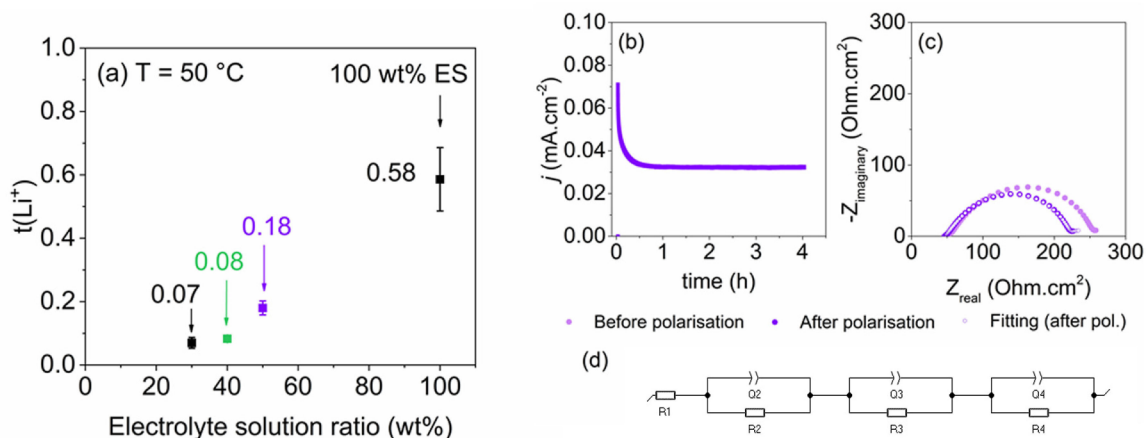


Figure 2. a) Lithium transference number for different ES ratios in PDADMA NTf₂ (30, 40, 50 and 100 wt%), including average values and standard deviations at 50 °C; b) Polarisation profile of a Li|Li symmetric cell containing 50/50-Al₂O₃ polymer composite electrolyte and reaching a steady state current ($\Delta V = 20 \text{ mV}$, $\Delta t = 4 \text{ h}$) at 50 °C; c) Nyquist plots of the cell before and after polarisation, fit to equivalent circuit shown in (d).

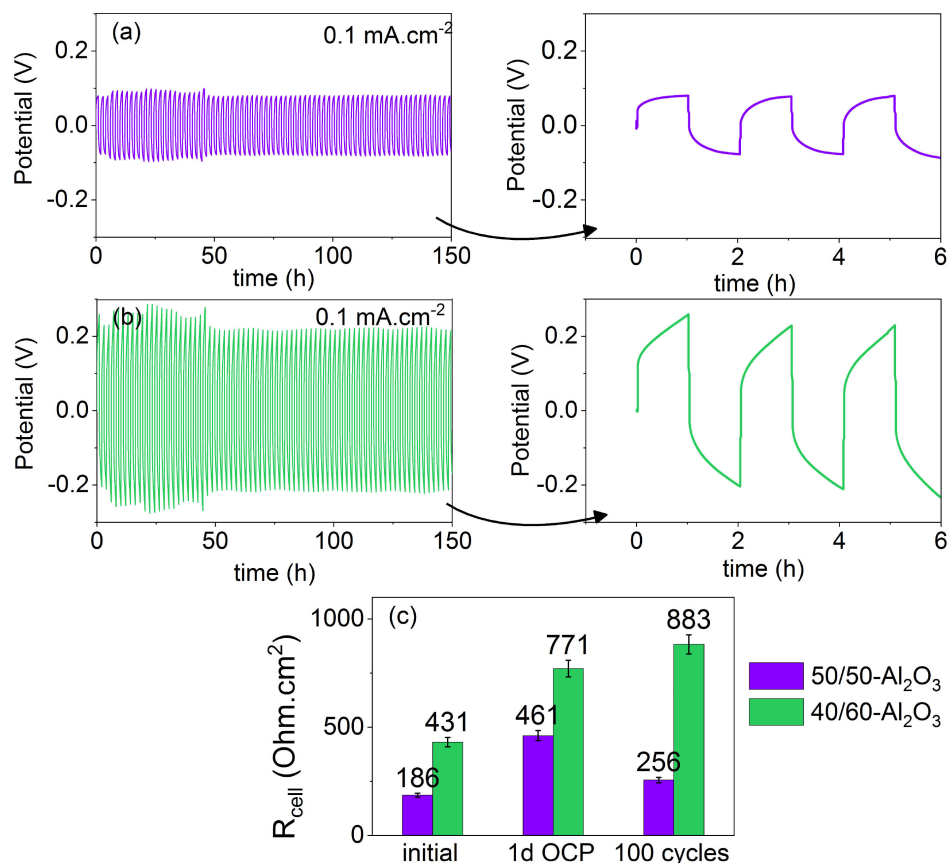


Figure 3. Voltage profiles during lithium plating/stripping processes in Li|Li symmetric cells containing different electrolytes at a current density $j = 0.1 \text{ mA cm}^{-2}$ ($q = 0.1 \text{ mAh cm}^{-2}$), at 50 °C a) 50/50-Al₂O₃, b) 40/60-Al₂O₃ polymer composite electrolytes; c) extracted cell resistance (R_{cell}) values post cell fabrication (initial), after 1 day under OCP and up to 100 lithium plating/stripping cycles at $j = 0.1 \text{ mA cm}^{-2}$ at 50 °C

and 50th stripping) for Li stripping. After decreasing the IL content in the electrolyte, the cell with 40/60-Al₂O₃ electrolyte, exhibits (Figure 3b) a higher voltage (≈ 0.26 ; 0.22 V at the first and 50th plating) for Li plating and a low voltage (≈ -0.20 ; -0.21 V at the first and 50th stripping) for Li stripping. Voltage

oscillations were more pronounced with the 40/60-Al₂O₃ electrolyte.

Another difference of note is the variation of the potential for each plating/stripping process. Generally, there are two processes during plating or stripping, the first rapid increase of potential corresponds to the total resistance of the bulk

electrolyte and electrolyte/electrode interface, the subsequent gradual increase of potential is attributed to the establishment of the concentration gradient through the cell.^[38] Based on our observations with both polymer composites, the increase of IL content can effectively lower the ohmic contribution and facilitates a faster equilibration of the concentration gradient (smaller slope), which is consistent with the conductivity and diffusion data from our previous report.^[14] Any small variation in the voltage is a fingerprint of differences in active surface areas on the Li-metal electrodes causing polarisation during the plating/stripping processes. A stable interface is characterised by minimal polarisation and high efficiency cycling performance. Therefore, a more stable interface was detected in the composite with highest IL content, that is 50/50-Al₂O₃ electrolyte. The results confirm a good contact between Li-metal and the polymer composite electrolyte; otherwise large currents would be accumulated at interfacial areas leading to significant cell polarisation.

The overall cell resistance encompassing the interfacial resistance and electrolyte resistance was evaluated by EIS. Extracted cell resistance (R_{cell}) values are given in Figure 3c at different intervals: post cell fabrication (initial), after 1 day under OCP and after 100 lithium plating/stripping cycles at $j=0.1\text{ mA cm}^{-2}$ at 50 °C. At all intervals, the cell resistance with the 40/60-Al₂O₃ electrolyte is about twice as large as that of with 50/50-Al₂O₃ electrolyte, suggesting a less resistive interface at the Li-metal electrode when the IL content is increased. When comparing the cell resistance prior to and after cycling, a significant decrease from 461 ± 23 to $256 \pm 13\text{ }\Omega\text{ cm}^2$ is noticed with the 50/50-Al₂O₃ electrolyte whereas the resistance increases slightly in the case of the 40/60-Al₂O₃ electrolyte (from 771 ± 39 to $883 \pm 44\text{ }\Omega\text{ cm}^2$). Overall based on these results an increase of IL content improves the compatibility with the Li-metal anode.

2.3. Plating/Stripping on Lithium-Metal in 50/50-Al₂O₃ Polymer Composite Electrolyte

From the results thus far, an investigation of the cycling performance of Li-metal in the electrolyte with the highest IL content, at higher current densities was undertaken. Figure 4a shows the time-dependent voltage profile of the Li|Li symmetric cells with the 50/50-Al₂O₃ electrolyte at a current density of 0.5 mA cm^{-2} at 50 °C, that is, a current density five times higher than the one discussed in the previous section. Extensive plating/stripping of Li-metal was demonstrated over 20 days, a significant amount of time of reversible plating/stripping processes, allowing one hour for each plating or stripping polarisation step. It is important to note that cycling of Li-metal in polymer composite at such current rates is more challenging than in liquid electrolytes due to slower kinetics and limited mass transport.^[2] The polarisations were also highly stable, $\approx 0.12\text{ V}$ maintained over 300 plating processes and $\approx -0.12\text{ V}$ maintained over 300 stripping processes. The constant symmetry in the values reflects a high coulombic efficiency and high reversibility in the electrochemical processes. The polar-

isation values were remarkably similar for 0.1 and 0.5 mAh cm^{-2} . A difference can be noted on the profile shape. A steady-state can be achieved faster when a low current density (i.e., 0.1 mA cm^{-2}) is applied whereas when the current density is increased to 0.5 mA cm^{-2} the equilibration time is extended by the slower dynamics as more charge carriers are needed.

Moreover, the Li-metal electrode surface impedance was monitored at intervals when the current density was varied, after the 'conditioning' step at 0.01 mA cm^{-2} and after 300 cycles at 0.5 mA cm^{-2} , and the Nyquist spectra are illustrated in Figure 4b.

A pronounced shift towards lower values of the second semi-circle touch down can be observed and is attributed to the resistance components arising from the interphases when electrode passivation occurs.^[39] This reflects the evolution of the SEI composition during cycling. The significant decrease of resistance post-cycling indicates again the low resistive nature of the interphases on the Li-metal surface and high compatibility of the 50/50-Al₂O₃ electrolyte with the Li electrode. The values of the corresponding bulk electrolyte resistance component (R_{bulk}) and resistance components arising from interphases ($R_{interphases}$) at different cycling intervals are plotted in Figure 4c. The observations confirm a slight decrease of bulk electrolyte resistance component, from 94 ± 5 to $55 \pm 3\text{ }\Omega\text{ cm}^2$, and an important decrease of the interphases resistance from $458 \pm 23\text{ }\Omega\text{ cm}^2$ to $246 \pm 12\text{ }\Omega\text{ cm}^2$ (when the current density is increased from 0.01 to 0.5 mA cm^{-2} respectively). Similar observations were recently reported for the same polyLL and the positive changes were assigned to the presence of mixed anions, NTf_2^- and FSI^- , within the electrolyte.^[17]

This phenomenon has previously been assigned to the protruding tips of 'fresh' deposited Li that offers a stronger electrical field and a higher specific surface area, resulting in a higher interface area with the polymer composite electrolyte and lower bulk and grain boundary resistances.^[28] The next section provides further insight into the surface morphology at the Li-metal/composite electrolyte interface.

2.4. Morphology of Lithium-Metal/Composite Electrolyte Interface Before and After Cycling

The surface morphology of the 50/50-Al₂O₃ composite electrolyte and the Li-metal/composite interface were further investigated by SEM. The surface morphology of the 50/50-Al₂O₃ electrolyte is presented before cycling (Figure 5a) and after cycling (Figure 5b). The features observed within the cross-section of the material prior to cycling could be ascribed to the entanglements between nanoparticles and the polymer backbones, which can account for the mechanical strength to the composite. These features are still observed after the electrolyte was submitted to 300 plating/stripping processes confirming the conservation of dimensional integrity and mechanical strength. No morphological sign of decomposition of the polymer composite post-cycling were identified. It should be noted that the 'breathable' structure of the polymer composite post-cycling (Figure 5b) can be attributed to the conduction

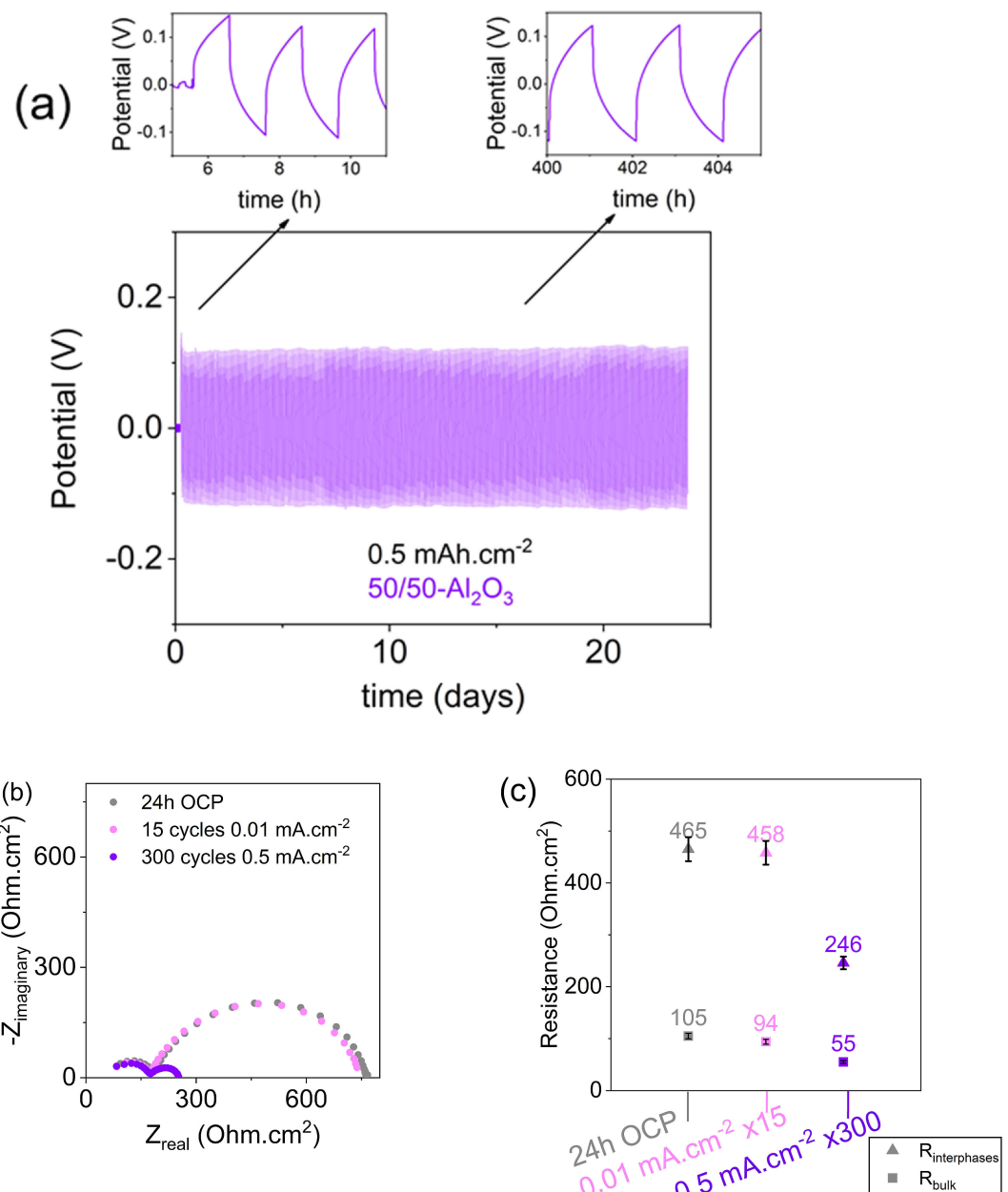


Figure 4. a) Voltage profiles during lithium plating / stripping processes in $\text{Li}|\text{Li}$ symmetric cells containing 50/50- Al_2O_3 polymer composite electrolyte at a current density $j = 0.5 \text{ mA cm}^{-2}$ ($q = 0.5 \text{ mAh cm}^{-2}$) at 50°C ; b) Nyquist spectra of the cell at different stages of cycling and c) corresponding bulk resistance component (R_{bulk}) and resistance components arising from interphases ($R_{\text{interphases}}$).

pathway established within the electrolyte. These observations are in agreement with the stable cycling performance previously described. The surface morphology of the $\text{Li}|50/50\text{-Al}_2\text{O}_3$ electrolyte interface is given at different magnifications in Figures 5c and d. The SEM observation is consistent with the effective performance observed during cycling; no visible sign of dendrite formation, i.e., no protrusions with high curvature, is evident.^[2] We attempted to identify the following separate regions: Li substrate, Li|electrolyte interface and polymer composite electrolyte, as illustrated in Figure 5c. Furthermore, in the presence of dendritic or mossy Li deposition, either a characteristic voltage decay associated with increased surface area and freshly exposed Li is typically observed, or erratic

voltage behaviour indicating fractal-like dendrite formation is expected.^[40] Instead we observed an initial decrease of the interfacial resistance (Figure 4) in the early cycles, typical for IL based electrolytes^[28,41–42] followed by a very stable and unchanging voltage-time profile. Based on the electrochemical results previously discussed and morphological analysis we believe that the SEI formed in contact with the 50/50- Al_2O_3 polymer composite electrolyte is the main reason for prohibited growth of lithium dendrite.

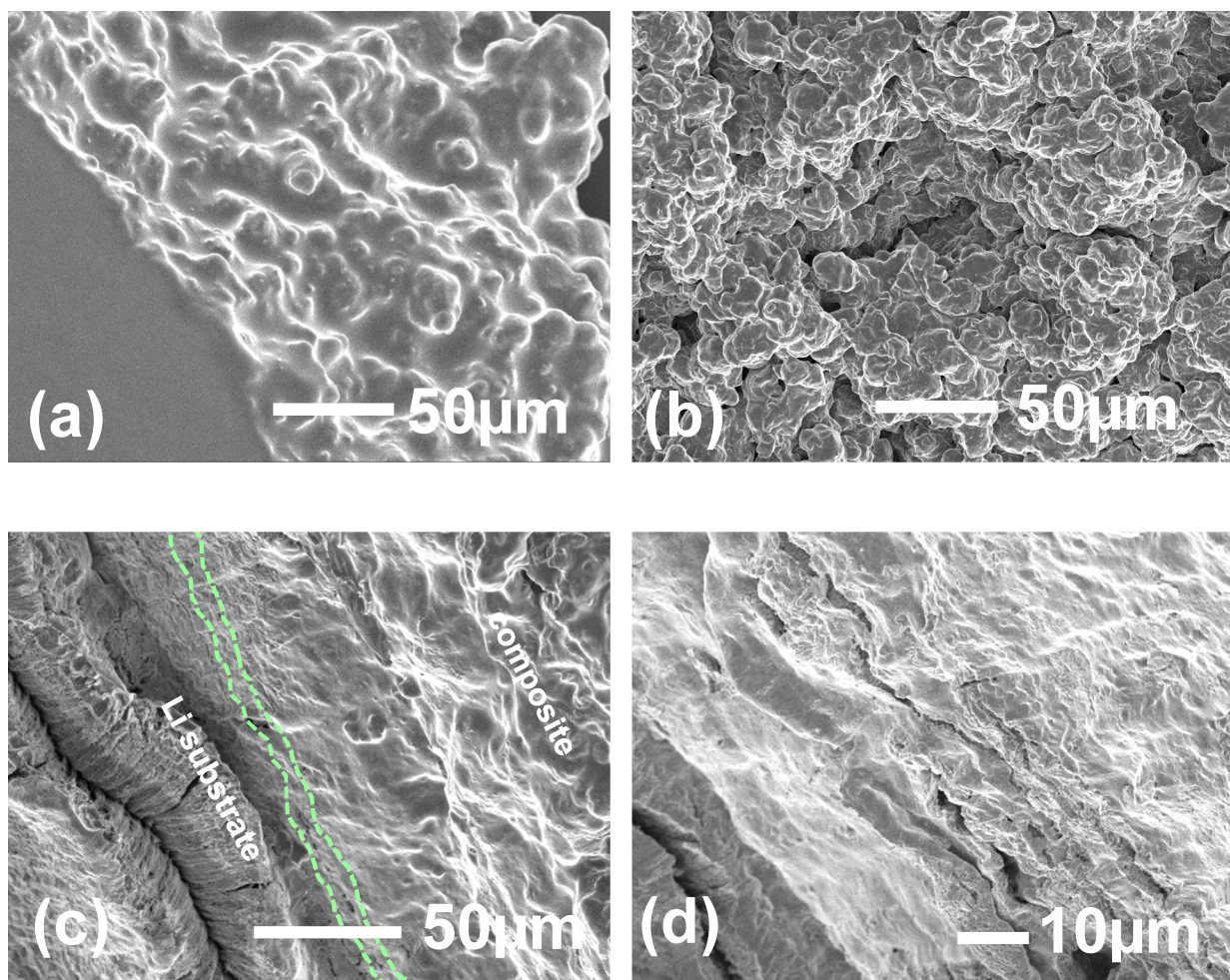


Figure 5. SEM images of 50/50-Al₂O₃ composite electrolyte before (a) and after 300 (b) plating/stripping processes at $j=0.5 \text{ mA cm}^{-2}$ ($q=0.5 \text{ mAh cm}^{-2}$) at 50 °C. (c) and (d) SEM images of lithium/electrolyte interface, Li|50/50-Al₂O₃ electrolyte after 300 plating/stripping processes at $j=0.5 \text{ mA cm}^{-2}$ ($q=0.5 \text{ mAh cm}^{-2}$) at 50 °C.

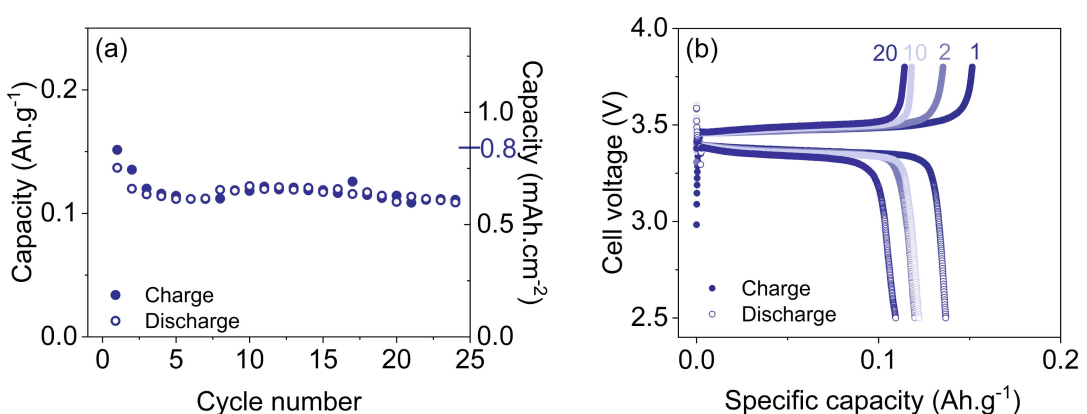


Figure 6. a) Cycling performance for Li|LFP cells containing 50/50-Al₂O₃ polymer composite electrolyte for 25 cycles at a current rate 0.07 C (C/15) and 50 °C, the capacity is given in Ah g⁻¹ (left axis) and mAh cm⁻² (right axis); b) corresponding charge-discharge profiles after 1, 2, 10 and 20 cycles. The active mass loading of LFP is 5.5 mg cm⁻² (i.e., 1.2 mAh cm⁻² based on a theoretical capacity of 170 mAh g⁻¹).

2.5. Performance of LiFePO₄ Electrodes

The 50/50-Al₂O₃ polymer composite electrolyte was tested in Li|LiFePO₄ batteries. Li|LiFePO₄ battery cycling for 25 cycles at

0.07 C (C/15) and 50 °C is presented in Figure 6a (capacity vs. cycle number). Figure 6b shows the voltage vs. capacity of selected charge and discharge cycles obtained at this rate. The 50/50-Al₂O₃ electrolyte exhibits an initial charge and discharge

capacity of 151 and 137 mAh g⁻¹ respectively. The capacity value obtained at initial charge is close to the theoretical capacity. A decrease in both charge and discharge capacity follows and it stabilises rapidly with slight oscillations between 110 and 120 mAh g⁻¹. The results suggest an irreversible loss after the second charging process, possibly arising from side reactions induced by the high LiFePO₄ content. The slight variations in capacity are likely due to SEI formation, penetration mechanism and contact of the IL component that control the amount of capacity, as reported in this type of electrolyte.^[17] The coulombic efficiency is 90% at the first cycle and rapidly increases to 98% at the 5th cycle. The discharge, i.e., Li insertion process, is evident with a well-defined single flat plateau at ca. 3.3–3.4 V. Reduced reactivity with electrolytes usually results in the very flat potentials during charge-discharge processes as seen in a typical Li|polymer|LiFePO₄ battery up to medium rates (ca. 0.5 C).^[43] It is worth noting that for stable cycling of solid-state batteries, areal capacities higher than 1.0 mAh cm⁻² remain a challenge in comparison with liquid electrolytes. Here we demonstrate the cycling of LiFePO₄ electrodes with initial capacity of 0.8 mAh cm⁻² in the 50/50-Al₂O₃ composite electrolyte containing a high Li⁺ content, 28 wt %.^[44] A comparison of this material with latest reports on solid polymer electrolytes of a similar type is provided in Table 2. The 50/50-Al₂O₃ composite electrolyte reveals itself as a competitive candidate with solid polymer electrolytes.^[45] The review indicates that the design of the electrode material to improve ionic conduction is critical to all solid-state battery performance with high areal capacities. The performance of other electrode materials such as LiNi_{1/3}Mn_{1/3}Co_{1/3}O₂ (NMC) and LiNi_{0.8}Co_{0.15}Al_{0.05}O₂ (NCA) is being assessed.

3. Conclusions

This work reports on the cycling performance of Li-metal electrodes in novel polymer composite electrolytes with polyIL host and mixed NTF₂⁻ and FSI⁻ anions, and helps establish guidelines for selecting and designing materials for effective Li-metal cycling. The incorporation of alumina nano-particles allows to finely tune the composite materials properties and find a balance between mechanical strength and integrity and transport properties. The choice of IL content within the composite material is critical to allow effective cycling of the Li-metal electrode. Reversible Li plating/stripping performance was assessed in the composite electrolytes. It was demonstrated that a saturated LiFSI solution in the P₁₁₁₁₄FSI phosphonium IL, when confined inside a PDADMA NTF₂ poly(ionic liquid) matrix, is compatible with Li-metal electrodes. The impact of an increase in IL content within the polymer composite electrolyte on the cyclability of Li-metal electrodes was analysed. The Li|Li symmetric cell with the highest IL content, that is 50 wt %, exhibited extensive reversible lithium plating/stripping with a current density of up to 0.5 mA cm⁻² for over 20 days and good adhesion to the Li-metal substrate was confirmed by impedance. SEM analysis of the electrolyte morphology and interface confirmed a stable performance and inhibited growth of lithium dendrites at the interface. The cycling of LiFePO₄ electrodes at C/15 was also demonstrated. This electrolyte is expected to be a promising candidate for high energy density Li-metal polymer batteries. Further electrochemical characterisation of polymer composite electrolytes, based on PDADMA FSI host with the same IL, is being carried out to effectively assess the impact of the anion chemistry on the electrolyte properties and performance of Li-metal electrodes.

Table 2. A comparison between the studied polymer composite electrolyte and other solid electrolytes against lithium iron phosphate positive electrode materials, i.e., LiFePO₄, considering a theoretical capacity of 170 mAh g⁻¹ for LiFePO₄.

IL	Polymer	Mass ratio [wt %] Li:IL:Polymer	Conditions (C-rate, T, E window vs. Li/Li ⁺)	Initial discharge capacity [mAh g ⁻¹]	Ref.
P ₁₁₁₁₄ FSI	PDADMA NTF ₂	0.28:0.22:0.50	0.07 C (C/15), 50 °C 2.5–3.8 V 0.1 C, 50 °C 2.6–3.9 V	137 (charge: 151) 50	This work
–	LiFSI/Jeffamine® M-2070	–	0.1 C, 80 °C 2.5–4.2 V	ca. 160	[17]
C ₄ mpyr FSI	PDADMA NTF ₂	0.08:0.37:0.55	0.1 C, 40 °C 2.0–4.0 V	144	[43]
C ₄ mpyr NTF ₂	PDADMA NTF ₂	0.12:0.60:0.28	0.1 C, 65 °C 2.5–4.0 V	ca. 125–130	[52]
EMI NTF ₂	f-SiO ₂ NFs	–	0.1 C, RT ^[a] 2.5–4.2 V	75.8	[53]
EMI NTF ₂	Si cross linked polymer (PEG + GPTMS)	X:0.70:1.0	0.1 C, RT ^[a] 2.7–4.2 V	ca. 60	[54]
–	poly(CL-co-TMC)-LiNTf ₂	–	0.1 C, 50 °C 2.6–3.9 V	50	[45]
–	LiFSI/Jeffamine® M-2070	–			

[a] RT: room temperature

Experimental Section

Materials

Trimethyl(isobutyl)phosphonium dimethylphosphate, $P_{1114}DMP$ (mixture with dimethylphosphoric acid, >99.5%, Cytec Solvay Canada) and potassium bis(fluorosulfonyl)imide, KFSI (>99.9%, Suzhou Fluolyte China) were used as received to synthesise trimethylisobutylphosphonium bis(fluorosulfonyl)imide, $P_{1114}FSI$.^[46] The electrolyte solution (ES) consisting of 3.8 moles of LiFSI per kg of $P_{1114}FSI$ (3.8 m) was prepared by dissolving the appropriate amount of lithium bis(fluorosulfonyl)imide, LiFSI salt (>99.9%, Coors Tek) in $P_{1114}FSI$ according to previous work.^[25] Poly(diallyldimethylammonium) bis(trifluoromethanesulfonyl)imide, PDADMA NTf₂, was synthesised by anion metathesis of poly(diallyldimethylammonium) chloride (20 wt% in H₂O, $M_w=400,000\text{--}500,000\text{ g mol}^{-1}$, Sigma Aldrich Australia) and lithium bis(trifluoromethanesulfonyl)imide, LiNTf₂ (>99%, Cors Tek US) in acetonitrile, CH₃CN (>99%, Lab supply Australia).^[47] 5 wt% of aluminium oxide nanoparticles, Al₂O₃ (0.05 μm, neutral activated Brockmann I grade, <0.03% Fe₂O₃, Sigma Aldrich Australia) was used to formulate the polymer composites. The chemical structures of the polyIL and the IL used to prepare the composites are given in Figure 1. The molar composition of each component in the formulated composites is provided in Table 1. Polymer composite electrolytes were prepared by solution casting method as described in our previous work and the final thickness of the polymer composite was 200 μm.^[14] For convenience, the prepared samples with Al₂O₃ are referred to as composite X/Y-Al₂O₃ electrolytes, where X/Y is the weight ratio of ES to PDADMA NTf₂ and the weight fraction of Al₂O₃ to ES and PDADMA NTf₂ is 5 wt%. The Al₂O₃ weight fraction was selected due to the favourable transport properties observed in other polymer/salt systems.^[48]

Lithium Cell Assembly and Characterisation

All cells were assembled inside an argon glove box according to the following procedure. CR2032-type cells were prepared by sandwiching the polymer composite electrolytes between two electrodes. The electrodes used to assemble Li|Li and Li|LiFePO₄ cells were as following: fresh Li-metal disks (8 mm in diameter, 100 μm thick, 99.9%, Sigma Aldrich Australia) brushed in hexane (>99%, Lab Supply Australia) and lithium iron phosphate, i.e., LiFePO₄, electrodes (8 mm in diameter, mass loading of 5.5 ± 0.1 mg cm⁻², i.e., 1.2 mAh cm⁻² Aleees). The LiFePO₄ electrode composition was 80 wt% LiFePO₄, 10 wt% PVDF (Solef 5130, Solvay) and 10 wt% conductive carbon (C65, Timcal). N-Methyl-2-pyrrolidone (99.5%, Sigma Aldrich Australia) was the solvent used to formulate the LiFePO₄ electrodes. The hexane solvent was distilled under rotary evaporation and dried on molecular sieves. The active area of the electrodes thus fabricated was ca. 0.5 cm². All cells were placed in an oven 1–2 hours after assembly, with a consistent period between assembly and transfer to ensure similar initial SEI properties. Cells were then stored for 24 hours at 50 °C inside the oven prior to commencement of the cycling experiments (Precision Compact, Thermo Scientific, ΔT = ±0.1 °C). The temperature was chosen strategically as the internal operating temperature of Li-metal polymer batteries sits between 50 and 80 °C.^[49]

The interfacial resistance evolution was monitored via electrochemical impedance spectroscopy (EIS) using a Multi Potentiostat VMP3 (Bio-Logic, France). The spectra were recorded between 0.1 Hz and 7 MHz with an amplitude of 5 mV. They were analysed with the EC-Lab software (Z Fit v. 11.12) and the impedance was reported within 5% error. The resulting impedance plot (Nyquist plot), $-Z_{\text{imaginary}}$ vs. Z_{real} on a complex plane, will consist of two or

three adjoining semicircles, depending on the relative magnitudes and characteristic frequencies of bulk electrolyte (R_{bulk}) and interphases ($R_{\text{interphases}}$) resistor components. Figure 2d schematically illustrates the equivalent electric circuit where all resistor components ($R_{\text{bulk}}=R_1$ and $R_{\text{interphases}}=R_2+R_3+R_4$) are well resolved.^[39] For EIS analysis, the Nyquist spectra start with the Ohmic resistance followed by one, or more semicircles at lower frequencies. The Ohmic part of the cell resistance is determined by the ionic conductivity of the electrolyte, R_{bulk} ; the following semicircle consequently corresponds to the processes at or on the two electrodes: capacitive properties of the grain boundary resistances in the SEI and the charge-transfer resistances at the Li electrodes. As these resistances occur at or on the surface of the Li electrodes (including the SEI), they are interpreted as 'Li electrode surface resistance' ($R_{\text{interphase}}$). In this report we chose to use the overall cell resistance $R_{\text{cell}}=R_{\text{bulk}}+R_{\text{interphases}}$ to measure all the resistances including the SEI.

Galvanostatic cycling tests were carried out using the Multi Potentiostat VMP3 at 50 °C ± 0.1 °C. For Li|Li cells, the amount of charge applied during each cycle (1 cycle: 1 'plating' + 1 'stripping' process) was consecutively 0.1 and 0.5 mAh cm⁻² with a 100 μm thick Li electrode. The current density for the Li-metal plating/stripping was respectively set at 0.1 and 0.5 mA cm⁻² (corresponding to 1 h 'charge' and 1 h 'discharge') with cutoff voltages of +0.5 V and -0.5 V vs. Li⁺/Li⁰. In each case a 'conditioning' step was used to allow smooth SEI formation on the Li-metal electrode (0.01 mA cm⁻² for 15 min 'charge' and 15 min 'discharge'). Li|LiFePO₄ cells were cycled between 2.5 and 3.8 V vs. Li⁺/Li⁰ at C/15 rate.

Chronoamperometry was used to determine the Li⁺ transference number, t_{Li}^{+} , for each electrolyte using a Li|polymer composite|Li cell setup. Alternating current (AC) impedance and direct current (DC) polarisation measurements were combined.^[13,36,50] This method, developed by Evans, Bruce and Vincent, consists of applying a constant voltage, and the resulting current is monitored as function of time, which allows a comparison between the effective charge carried and the applied charge. t_{Li}^{+} is determined by measuring the initial and steady state currents and the resistances of the electrode surface before and after polarisation. A steady state is reached after a certain time when only the Li⁺ cation moves towards the negatively polarised electrode. By taking into consideration the growing passivation layer at the electrode as a consequence of the reaction between the electrolyte and the freshly deposited Li crystal on the anode, and the concentration gradient, Watanabe demonstrated that the Li⁺ transference number in a polymer electrolyte can be calculated by the following equation using a symmetric cell setup [Eq. (1)].^[51]

$$t_{\text{Li}}^{+} = \frac{R_{\text{BS}}}{(\frac{\Delta V}{I_s} - R_{\text{IS}})} \quad (1)$$

where ΔV is the d.c. potential applied across the cell, I_s is the current reached in the steady-state for sample polarised with d.c. bias, R_{BS} and R_{IS} are the resistances of bulk and SEI respectively after d.c. polarisation. The cells were polarised at 50 °C with a constant voltage of 20 mV for 4 hours and the currents were measured during the polarisation. EIS spectra were acquired before and after the polarisation using a perturbation amplitude of 1 mV (7 MHz to 0.1 Hz). A 24-hour resting period was allowed between each measurement.

Scanning Electron Microscopy

In order to investigate the morphology of the post-cycling deposition and the interface between the electrolyte and Li-metal,

cycled coin cells were disassembled to recover Li-metal disks for further post-cycling characterisation by scanning electron microscopy (SEM). Cross-section images of the electrolytes and their interface with Li-metal were obtained with a JEOL JSM-IT300 at an accelerating voltage of 2 kV. Cross-section of the interface was prepared by cutting the Li electrodes with a surgical blade. To avoid electrode contamination or side reactions of the Li electrodes with atmospheric moisture and oxygen, the samples were transferred from the glove box to the SEM in a sealed stainless-steel vessel filled with Argon. The vessel was introduced into the SEM via a purpose designed load-lock chamber for loading air-sensitive samples.

Abbreviations

P ₁₁₁₄ FSI	trimethyl(isobutyl)phosphonium bis(fluorosulfonyl)imide
PDADMA NTf ₂	poly(diallyldimethylammonium) bis(trifluoromethanesulfonyl)imide
ES	electrolyte solution
3.8 mol kg ⁻¹ of LiFSI in X/Y-Al ₂ O ₃ composite, polymer composite	X/Y-Al ₂ O ₃ composite, polymer composite electrolyte with X wt % ES/Y wt %
P ₁₁₁₄ FSI	PDADMA NTf ₂ and 5 wt % Al ₂ O ₃

Acknowledgements

The authors would like to acknowledge the support of the Australia-India Strategic Research Fund (AISRF, grant agreement No. 48515). Prof. Maria Forsyth and Douglas MacFarlane thank the Australian Research Council for the Australian Laureate Fellowship programs. The authors also thank the Battery Technology Research and Innovation Hub (BatTRI-Hub) at Deakin University for their battery prototyping facilities.

Conflict of Interest

The authors declare no conflict of interest.

Keywords: ion transport • lithium-metal • PDADMA • phosphonium ionic liquids • polymer composite

- [1] D. R. MacFarlane, M. Forsyth, P. C. Howlett, M. Kar, S. Passerini, J. M. Pringle, H. Ohno, M. Watanabe, F. Yan, W. Zheng, S. Zhang, J. Zhang, *Nat. Rev. Mater.* **2016**, *1*, 15005.
- [2] D. Lin, Y. Liu, Y. Cui, *Nat. Nanotechnol.* **2017**, *12*, 194–206.
- [3] Q. Li, J. Chen, L. Fan, X. Kong, Y. Lu, *Green Energy & Environment* **2016**, *1*, 18–42; *Environment* **2016**, *1*, 18–42.
- [4] A. Mauger, M. Armand, C. M. Julien, K. Zaghib, *J. Power Sources* **2017**, *353*, 333–342.
- [5] M.-A. Néouze, J. Le Bideau, P. Gaveau, S. Bellayer, A. Vioux, *Chem. Mater.* **2006**, *18*, 3931–3936.
- [6] S. Sen, S. Malunavar, A. J. Bhattacharyya, *J. Phys. Chem. B* **2016**, *120*, 10153–10161.
- [7] H. Shobukawa, H. Tokuda, M. A. B. H. Susan, M. Watanabe, *Electrochim. Acta* **2005**, *50*, 3872–3877.
- [8] R. Bhandary, M. Schönhoff, *Electrochim. Acta* **2015**, *174*, 753–761.
- [9] M. A. B. H. Susan, T. Kaneko, A. Noda, M. Watanabe, *J. Am. Chem. Soc.* **2005**, *127*, 4976–4983.
- [10] S. N. F. Yusuf, R. Yahya, A. K. Arof, in *Progress and Developments in Ionic Liquids* (Ed.: S. Handy), InTech, Rijeka, **2017**, p. Ch. 08.
- [11] M. Salsamendi, L. Rubatat, D. Mecerreyes, in *Electrochemistry in Ionic Liquids* (Ed.: A. A. J. Torriero), Springer International Publishing, **2015**, pp. 283–315.
- [12] J. Le Bideau, L. Viau, A. Vioux, *Chem. Soc. Rev.* **2011**, *40*, 907–925.
- [13] A. Guyomard-Lack, B. Said, N. Dupré, A. Galarneau, J. Le Bideau, *New J. Chem.* **2016**, *40*, 4269–4276.
- [14] X. Wang, H. Zhu, G. Girard, R. Yunis, D. MacFarlane, D. Mecerreyes, A. Bhattacharyya, P. C. Howlett, M. Forsyth, *J. Mater. Chem. A* **2017**, *5*, 23844–23852.
- [15] A. S. Shaplov, R. Marcilla, D. Mecerreyes, *Electrochim. Acta* **2015**, *175*, 18–34.
- [16] J. L. Pablos, N. García, L. Garrido, J. Guzmán, F. Catalina, T. Corrales, P. Tiemblo, *J. Membr. Sci.* **2018**, *545*, 133–139.
- [17] M. Kerner, P. Johansson, *Batteries* **2018**, *4*, 10.
- [18] G. B. Appetecchi, G. T. Kim, M. Montanino, M. Carewska, R. Marcilla, D. Mecerreyes, I. De Meatz, *J. Power Sources* **2010**, *195*, 3668–3675.
- [19] J. L. Pablos, N. García, L. Garrido, F. Catalina, T. Corrales, P. Tiemblo, *J. Mater. Chem. A* **2018**, *6*, 11215–11225.
- [20] Q. Guo, Y. Han, H. Wang, X. Hong, C. Zheng, S. Liu, K. Xie, *RSC Adv.* **2016**, *6*, 101638–101644.
- [21] Y. S. Yun, S.-W. Song, S.-Y. Lee, S.-H. Kim, D.-W. Kim, *Curr. Appl. Phys.* **2010**, *10*, e97–e100.
- [22] C. Sun, J. Liu, Y. Gong, D. P. Wilkinson, J. Zhang, *Nano Energy* **2017**, *33*, 363–386.
- [23] A. I. Bhatt, I. May, V. A. Volkovich, M. E. Hetherington, B. Lewin, R. C. Thied, N. Ertok, *J. Chem. Soc. Dalton* **2002**, 4532–4534.
- [24] K. Tsunashima, M. Sugiya, *Electrochim. Commun.* **2007**, *9*, 2353–2358.
- [25] G. M. A. Girard, M. Hilder, H. Zhu, D. Nucciarone, K. Whitbread, S. Zavorine, M. Moser, M. Forsyth, D. R. MacFarlane, P. C. Howlett, *Phys. Chem. Chem. Phys.* **2015**, *17*, 8706–8713.
- [26] M. Hilder, G. M. A. Girard, K. Whitbread, S. Zavorine, M. Moser, D. Nucciarone, M. Forsyth, D. R. MacFarlane, P. C. Howlett, *Electrochim. Acta* **2016**, *202*, 100–109.
- [27] M. Chen, B. Tyler White, C. R. Kasprzak, T. E. Long, *Eur. Polym. J.* **2018**, *1*.
- [28] G. M. A. Girard, M. Hilder, D. Nucciarone, K. Whitbread, S. Zavorine, M. Moser, M. Forsyth, D. R. MacFarlane, P. C. Howlett, *J. Phys. Chem. C* **2017**, *121*, 21087–21095.
- [29] G. M. A. Girard, M. Hilder, N. Dupre, D. Guyomard, D. Nucciarone, K. Whitbread, S. Zavorine, M. Moser, M. Forsyth, D. R. MacFarlane, P. C. Howlett, *ACS Appl. Mater. Interfaces* **2018**, *10*, 6719–6729.
- [30] N. Nitta, F. Wu, J. T. Lee, G. Yushin, *Mater. Today* **2015**, *18*, 252–264.
- [31] L. M. Suo, Y. S. Hu, H. Li, M. Armand, L. Q. Chen, *Nat. Commun.* **2013**, *4*.
- [32] W. Xu, J. L. Wang, F. Ding, X. L. Chen, E. Nasybutin, Y. H. Zhang, J. G. Zhang, *Energy Environ. Sci.* **2014**, *7*, 513–537.
- [33] X.-B. Cheng, R. Zhang, C.-Z. Zhao, F. Wei, J.-G. Zhang, Q. Zhang, *Adv. Sci.* **2016**, *3*.
- [34] J. Zhao, L. Wang, X. He, C. Wan, C. Jiang, *J. Electrochem. Soc.* **2008**, *155*, A292–A296.
- [35] S. Zugmann, M. Fleischmann, M. Amereller, R. M. Gschwind, H. D. Wiemhofer, H. J. Gores, *Electrochim. Acta* **2011**, *56*, 3926–3933.
- [36] P. G. Bruce, M. T. Hardgrave, C. A. Vincent, *Solid State Ionics* **1992**, *53*, 1087–1094.
- [37] G. Bielek, M. Winter, P. Bielek, *Phys. Chem. Chem. Phys.* **2015**, *17*, 8670–8679.
- [38] M. Rosso, C. Brissot, A. Teyssot, M. Dollé, L. Sannier, J.-M. Tarascon, R. Bouchet, S. Lascaud, *Electrochim. Acta* **2006**, *51*, 5334–5340.
- [39] C. A. Lundgren, K. Xu, T. R. Jow, J. Allen, S. S. Zhang, in *Springer Handbook of Electrochemical Energy* (Eds.: C. Breitkopf, K. Swider-Lyons), Springer Berlin Heidelberg, Berlin, Heidelberg, **2017**, pp. 449–494.
- [40] K. N. Wood, M. Noked, N. P. Dasgupta, *ACS Energy Lett.* **2017**, *2*, 664–672.
- [41] L. Grande, J. von Zamory, S. L. Koch, J. Kalhoff, E. Paillard, S. Passerini, *ACS Appl. Mater. Interfaces* **2015**, *7*, 5950–5958.
- [42] A. I. Bhatt, P. Kao, A. S. Best, A. F. Hollenkamp, *J. Electrochim. Soc.* **2013**, *160*, A1171–A1180.
- [43] G. B. Appetecchi, G. T. Kim, M. Montanino, M. Carewska, R. Marcilla, D. Mecerreyes, I. De Meatz, *J. Power Sources* **2010**, *195*, 3668–3675.
- [44] J. Kasemchainan, P. G. Bruce, *Johnson Matthey Technol. Rev.* **2018**, *62*, 177.
- [45] I. Aldalur, M. Martinez-Ibañez, M. Piszzcz, L. M. Rodriguez-Martinez, H. Zhang, M. Armand, *J. Power Sources* **2018**, *383*, 144–149.
- [46] D. Nucciarone, S. I. Zavorine, K. M. Whitbread, M. Moser, in *European Patent Office, Vol. EP2952518* (Ed.: E. P. Office), **2015**.

- [47] A.-L. Pont, R. Marcilla, I. De Meatza, H. Grande, D. Mecerreyes, *J. Power Sources* **2009**, *188*, 558–563.
- [48] S. Das, A. Ghosh, *J. Appl. Phys.* **2015**, *117*, 174103.
- [49] H. Berg, *Batteries for Electric Vehicles: Materials and Electrochemistry*, Cambridge University Press, Cambridge, **2015**.
- [50] J. Evans, C. A. Vincent, P. G. Bruce, *Polymer* **1987**, *28*, 2324–2328.
- [51] M. Watanabe, S. Nagano, K. Sanui, N. Ogata, *Solid State Ionics* **1988**, *28–30*, 911–917.
- [52] T. Yuuki, Y. Konosu, M. Ashizawa, T. Iwahashi, Y. Ouchi, Y. Tominaga, R. Ooyabu, H. Matsumoto, H. Matsumoto, *ACS Omega* **2017**, *2*, 835–841.
- [53] D.-J. You, Z. Yin, Y.-k. Ahn, S. Cho, H. Kim, D. Shin, J. Yoo, Y. S. Kim, *J. Ind. Eng. Chem.* **2017**, *52*, 1–6.
- [54] J. Mindemark, B. Sun, E. Törmä, D. Brandell, *J. Power Sources* **2015**, *298*, 166–170.

Manuscript received: November 8, 2018

Revised manuscript received: December 20, 2018

Version of record online: January 18, 2019
